# Deformed rotational bands in the doubly odd nuclei $^{134}$Pr and $^{132}$Pr

K. Hauschild, R. Wadsworth, R. M. Clark, and I. M. Hibbert
*Department of Physics, University of York, Heslington, York YO1 5DD United Kingdom*

C. W. Beausang, S. A. Forbes, P. J. Nolan, E. S. Paul, A. T. Semple, and J. N. Wilson
*Oliver Lodge Laboratory, University of Liverpool, Liverpool L69 3BX United Kingdom*

A. Gizon, J. Gizon, and D. Santos
*Institut des Sciences Nucléaires, Institut National de Physique Nucléaire et de Physique des Particules, Centre National de la Recherche Scientifique, Université Joseph-Fourier, 53 Avenue des Martyrs, 38026 Grenoble, France*

J. Simpson
*Nuclear Structure Facility, Daresbury Laboratory, Daresbury, Warrington WA4 4AD, United Kingdom*
(Received 24 March 1994)

The nuclei $^{132,134}$Pr have been investigated using the $^{100}$Mo($^{37}$Cl,$xn$) reactions at a beam energy of 155 MeV. Gamma rays were detected with the Eurogam array. Analysis of the data has revealed the presence of two new weakly populated decoupled bands in $^{134}$Pr. One of these bands has been linked into the normal-deformed states and is thought to be built on a $\pi(h_{11/2})^3 \otimes \nu(f_{7/2},h_{9/2})$ configuration. The second band has been interpreted as being based on a $\pi(h_{11/2})^3 \otimes \nu i_{13/2}$ intruder configuration within the second $\beta_2 \simeq 0.3$ prolate minimum. The known decoupled band in $^{132}$Pr ($5n$ reaction channel) and the highly deformed band in $^{130}$La ($\alpha 3n$) have also been extended. The structure of all of these bands is discussed together with similar bands in neighboring odd-odd nuclei.

PACS number(s): 27.60.+j, 23.20.Lv, 21.10.Re, 21.60.Ev

## I. INTRODUCTION

Highly deformed rotational bands have been observed in several nuclei around the $Z$=58, $N$=74 prolate subshell closures. These nuclei are prolate-deformed rotors with $\beta_2 \simeq 0.3$–0.4, corresponding to a major to minor axis ratio of approximately 3:2. The properties of highly deformed bands are strongly dependent on the occupancy of a few high-$j$ orbitals. In the mass $A \simeq 130$ region, the occupation of the $\nu i_{13/2}$ $[660]\frac{1}{2}^+$ Nilsson intruder orbital plays a dominant role in driving the nuclear core towards a large prolate deformation [1]. In the odd-$N$ nuclei, cranked shell model and total Routhian surface (TRS) calculations [1] indicate that the yrast bands within the highly deformed second minimum should have at least one $i_{13/2}$ neutron orbital occupied, while in even-$N$ nuclei two $i_{13/2}$ orbitals are occupied. It is therefore expected that even-even nuclei should be more deformed than the odd-$A$ nuclei. This is borne out experimentally; for example, the quadrupole deformations for the cerium isotopes $^{131}$Ce and $^{132}$Ce have been determined from mean lifetime measurements to be $\beta_2$=0.35 [2] and $\beta_2$=0.40 [3], respectively.

The feedout of the highly deformed bands in this mass region has two distinct characteristics. In the heavier $Z$ nuclei (i.e., $^{133,135}$Nd [4,5], $^{135,137,139}$Sm [6–8], and $^{141}$Gd [9]), transitions linking rotational bands into the normal-deformed states have been observed; however this is not the case for the nuclei $^{130}$La [10], $^{131,132}$Ce [11,12], and $^{134,136,137}$Nd [13,14]. For the Nd-Gd nuclei, TRS calculations indicate that the first energy minimum gradually evolves towards higher deformations with increasing spin (i.e., no real barrier). In contrast, for the La, Ce, and Pr nuclei, TRS calculations predict a second well-deformed minimum which is distinctly separated from the normal-deformed minimum by a large well-defined potential barrier. It is therefore expected that deexcitation from the second minimum to the normal-deformed states occurs through quantum tunneling. This results in a highly fragmented deexcitation process making it extremely difficult to observe any linking transitions.

An experiment has been performed using the Eurogam detector array [15–17] to investigate the high-spin states of the isotopes $^{132,133,134}$Pr. This experiment has revealed multiple highly deformed bands in $^{133}$Pr [18] and two new weakly populated decoupled bands in $^{134}$Pr. This paper presents the evidence for these two bands in doubly odd $^{134}$Pr. One of these bands, which has also been partially observed by Petrache *et al.* [19], and later extended [20] in experiments run concurrently with our own, is thought to arise from the population of $\nu h_{9/2}$ and $\pi h_{11/2}$ orbitals. The present work extends this band to even higher spin. The second band is interpreted as arising from the occupation of $\nu i_{13/2}$ and $\pi h_{11/2}$ orbitals. The present work has also significantly extended the known decoupled band in $^{132}$Pr [21]. In addition, two transitions, of energies 1513 and 1622 keV, have been added to the top of the previously known highly deformed band in $^{130}$La [10]. These results are compared with those obtained for other decoupled bands in neighbor-

 

ing odd-odd nuclei. Comparisons have also been carried out with cranked Woods–Saxon calculations [22,23] and total Routhian surface (TRS) calculations [1,24].

## II. EXPERIMENTAL DETAILS AND DATA ANALYSIS

High-spin states in $^{137-x}$Pr were populated by the $^{100}$Mo($^{37}$Cl,$xn$) fusion-evaporation reaction at a beam energy of 155 MeV. The beam, provided by the tandem Van de Graaff accelerator at the Nuclear Structure Facility, Daresbury Laboratory, was incident upon a 550 $\mu$g cm$^{-2}$ enriched $^{100}$Mo self-supporting target. Coincident gamma rays emitted during the decay of these high-spin states were detected with the Eurogam (phase I) array which, for this experiment, consisted of 41 large-volume HPGe Compton escape-suppressed detectors [15–17]. Approximately $7\times10^8$ events were recorded with an unsuppressed fold $\geq$ 8 which corresponds to $3.4\times10^9$ unpacked suppressed triples. The $^{134}$Pr channel was enhanced by demanding that one of these $\gamma$ rays was an uncontaminated low-lying transition in $^{134}$Pr. The remaining two coincident $\gamma$ rays were then incremented into an $E_{\gamma1}$-$E_{\gamma2}$ matrix which had approximately $500\times10^6$ events. A similar gated $E_{\gamma1}$-$E_{\gamma2}$ matrix was also produced to enhance the $^{132}$Pr ($5n$) reaction channel. The triples data were also sorted into an $E_{\gamma1}$-$E_{\gamma2}$-$E_{\gamma3}$ cube as well as being unpacked into doubles and sorted into a standard doubles matrix which contained $4.5\times10^9$ events. The more intense of the two bands in $^{134}$Pr (band 1) was cleanly selected using fourfold (and higher) coincidence events and requiring that a pair of $\gamma$ rays had energies that corresponded to members of the band. The other pair of $\gamma$ rays was then incremented into a standard $E_{\gamma1}$-$E_{\gamma2}$ matrix which was used for the subsequent analysis. To enhance band 2 in $^{134}$Pr, a gated $E_{\gamma1}$-$E_{\gamma2}$ matrix was produced using threefold (and higher) coincidence events by requiring that a single $\gamma$ ray had an energy which corresponded to that of a known band member. The remaining pair of $\gamma$ rays was then incremented into a standard $E_{\gamma1}$-$E_{\gamma2}$ matrix.

Measurements of angular intensity ratios were used to establish the multipolarities of $\gamma$-ray transitions. From the Eurogam data, matrices were sorted which contained $\gamma$-$\gamma$ coincidences from detectors at $\theta$=134° (10 detectors) and $\overline{90}^\circ$ (5 detectors at $\theta$=86° plus 5 detectors at $\theta$=94°) where $\theta$ is defined relative to the beam axis. From this matrix, it was possible to project out spectra gated by $\gamma$ rays at 134° and $\overline{90}^\circ$ and measure the intensities of other coincident $\gamma$ rays detected at $\overline{90}^\circ$ and 134°, respectively. This allowed the angular intensity ratio $I(134^\circ\text{–}\overline{90}^\circ)$ $/I(\overline{90}^\circ\text{–}134^\circ)$ to be deduced for each gamma-ray transition. These intensity ratios were compared with measured values of known stretched quadrupole $\leftrightarrow$ stretched quadrupole and stretched quadrupole $\leftrightarrow$ stretched dipole transitions, which were found to be 1.0 and 0.7, respectively. The values were used to assist with the assignment of the transition multipolarities using the method of directional correlation from oriented states (DCO) [25].

## III. RESULTS

Analysis of the present data has revealed two weakly populated decoupled bands which have been assigned to $^{134}$Pr from observed coincidence relationships with low-spin yrast transitions in $^{134}$Pr [26]. It has also led to the extension of the known decoupled band in $^{132}$Pr [21] by seven transitions, and the highly deformed band in $^{130}$La [10] by two transitions. Figure 1 shows $\gamma$-ray spectra for the two bands in $^{134}$Pr as well as the band in $^{132}$Pr. Figure 1(a) is derived from fourfold coincidence data and shows a summation of gates on a double-gated $E_{\gamma1}$-$E_{\gamma2}$ matrix for the more intensely populated band observed in $^{134}$Pr (band 1). All transitions of the band were used as gates to construct this spectrum. The weaker of the two bands observed in $^{134}$Pr (band 2) is shown in Fig. 1(b). This spectrum is a sum of $\gamma$-ray coincidence spectra obtained from the triples data using a single $\gamma$-gated $E_{\gamma1}$–$E_{\gamma2}$ matrix. The sum of gates on a single $\gamma$-gated $\gamma$-$\gamma$ matrix for the extended band in $^{132}$Pr is shown in Fig. 1(c). The insets of Fig. 1 illustrate more clearly the band members at higher spin. The intensities of the strongest transitions in band 1 and band 2, relative to the $^{134}$Pr reaction channel, were measured to be approximately 4% and 2%, respectively, and it is estimated that the decoupled band in $^{132}$Pr accounts for 5% of the $^{132}$Pr reaction channel. The transition energies, relative intensities (corrected for detector efficiency and internal conversion [27]), and DCO results for both bands in $^{134}$Pr, and the decoupled band in $^{132}$Pr, are given in Table I, while the DCO measurements for the linking transitions (see below) for band 1 in $^{134}$Pr and the decoupled band in $^{132}$Pr are given in Table II.

The high selectivity obtained using quadruples data has enabled band 1 to be linked into the known normal-deformed states of $^{134}$Pr. The band appears to decay out over the lowest two observed states as indicated by the relative in-band intensities shown in Table I. The linking transitions can be seen in the spectrum obtained from the double-gated $E_{\gamma1}$-$E_{\gamma2}$ correlation matrix [Fig. 1(a)]. When gated by the 458 keV ($10^+ \rightarrow 8^+$) transition, the DCO ratios (Table II) for the 211, 245, and 339 keV transitions are consistent with stretched quadrupole $\leftrightarrow$ stretched dipole correlations, while the 611 and 645 keV transitions have DCO ratios consistent with stretched quadrupole $\leftrightarrow$ stretched quadrupole correlations. Thus the 211, 245, and 339 keV transitions are assigned as stretched dipoles, while the 611 and 645 keV transitions are assigned as stretched quadrupoles ($E2$). Having established that the 645 keV transition has a quadrupole nature it was possible to show that the DCO ratios for the remaining transitions within band 1 are consistent with stretched quadrupole $\leftrightarrow$ stretched quadrupole correlations. Figure 2(a) shows a background subtracted gate set on the 611 keV transition in the double-gated $E_{\gamma1}$-$E_{\gamma2}$ matrix. This spectrum indicates that the 339 and 245 keV linking transitions together with band 1, except the 645 keV transition, are in coincidence with the 611 keV $\gamma$ ray. Similarly, Fig. 2(b), which is a background subtracted spectrum gated on the 645 keV transition, shows that the 339 and 211 keV linking transitions

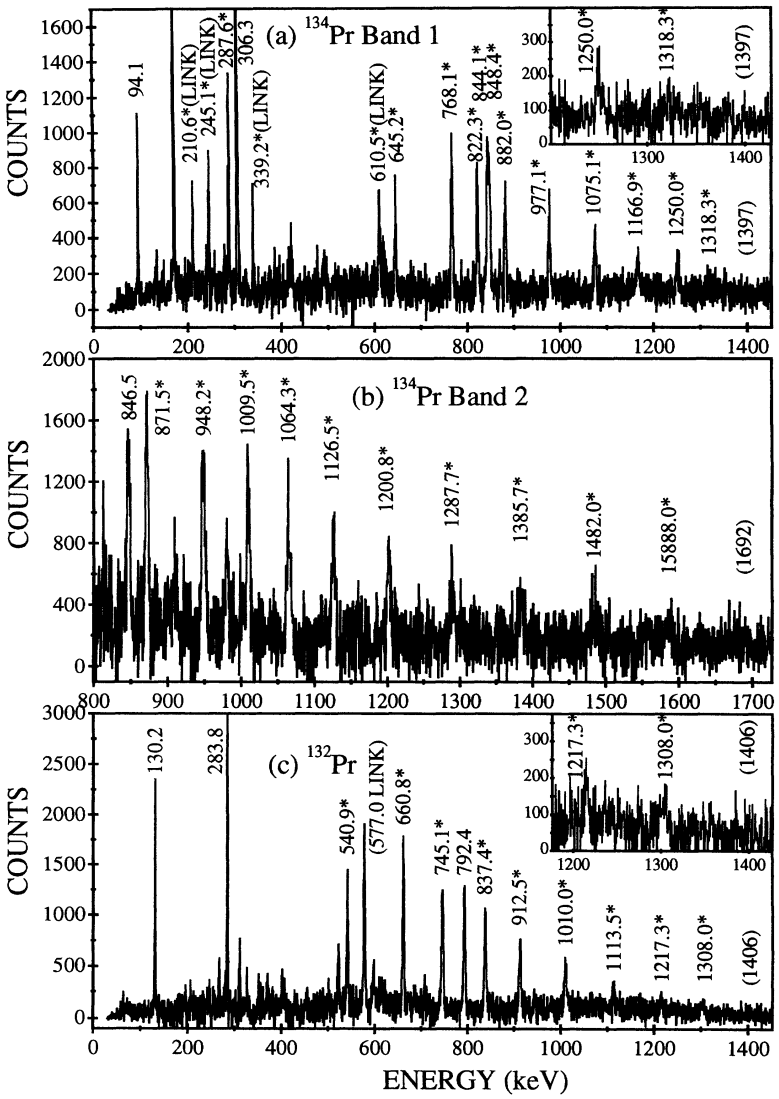


FIG. 1. Examples of gated coincidence spectra. Gates are indicated by an asterisk, LINK indicates a transition that links the band and the low-lying states and the $\gamma$-ray energies are labeled in keV. The insets more clearly show the band members at high spin. (a) A sum of gates on a double-gated $E_{\gamma 1}$-$E_{\gamma 2}$ matrix spectrum derived from fourfold coincidence data for the more intensely populated band in $^{134}$Pr (band 1). (b) A coincidence spectrum obtained from triples data of a sum of gates on a single-gated $E_{\gamma 1}$-$E_{\gamma 2}$ matrix for band 2 in $^{134}$Pr. (c) The sum of gates on a single-gated $E_{\gamma 1}$-$E_{\gamma 2}$ matrix derived from threefold coincidence data for the decoupled band in $^{132}$Pr.

are in coincidence with the 645 keV gate. The transitions labeled C in this spectrum are contaminants from an oblate band in $^{133}$Ce brought in by the 645 keV gate [28,29]. The level scheme showing the decay path of band 1 in $^{134}$Pr, deduced from the present work, is presented in Fig. 3. Not all the intensity of band 1 is accounted for, therefore Fig. 3 does not show the complete decay path. For example, only ~80% of the intensity of the 767 keV transition in band 1 feeds into the 611 and 645 keV transitions. Furthermore, less than half the intensity of the 611 keV linking transition, and a third of the 645 keV transition intensity is accounted for by the decay path

TABLE I. Gamma-ray energies, relative intensities (corrected for detector efficiency and electron internal conversion and normalized to the strongest transitions in each band), and angular correlation data for transitions in bands 1 and 2 in $^{134}$Pr and the decoupled band in $^{132}$Pr. Dashed lines indicate that a measurement was not possible through either contamination or low statistics.

| $^{134}$Pr band 1 | | | $^{134}$Pr band 2 | | | $^{132}$Pr decoupled band | | |
|---|---|---|---|---|---|---|---|---|
| $E_\gamma$ (keV) | Relative intensity | DCO ratio | $E_\gamma$ (keV) | Relative intensity | DCO ratio | $E_\gamma$ (keV) | Relative intensity | DCO ratio |
| 645.2(2) | 0.35(2) | 1.03(8) | 871.5(2) | 0.87(6) | - | 540.9(2) | 0.66(3) | 1.28(10) |
| 768.1(2) | 1.00(6) | 1.03(6) | 948.2(2) | 1.00(7) | 0.99(8) | 660.8(2) | 1.00(4) | 0.92(5) |
| 848.4(2) | 0.91(5) | - | 1009.5(2) | 0.87(7) | 1.04(10) | 745.1(2) | 0.80(3) | 1.00(7) |
| 822.3(2) | 0.81(5) | 0.89(5) | 1064.3(2) | 0.77(7) | 0.99(10) | 792.4(2) | 0.80(4) | 1.10(7) |
| 844.1(2) | 0.82(5) | - | 1126.5(2) | 0.61(5) | 0.94(16) | 837.4(2) | 0.58(3) | - |
| 882.0(2) | 0.76(4) | - | 1200.8(2) | 0.43(4) | 0.96(27) | 912.5(2) | 0.57(2) | - |
| 977.1(2) | 0.48(5) | 1.05(9) | 1287.7(2) | 0.38(4) | - | 1010.0(2) | 0.42(2) | - |
| 1075.1(2) | 0.40(3) | 0.96(9) | 1385.7(2) | 0.34(3) | - | 1113.5(2) | 0.24(2) | - |
| 1166.9(2) | 0.33(3) | - | 1482.0(2) | 0.17(2) | - | 1217.3(2) | 0.08(1) | - |
| 1250.0(2) | 0.24(2) | - | 1588.0(2) | 0.09(2) | - | 1308.0(2) | - | - |
| 1318.3(2) | 0.10(2) | - | 1692(1) | - | - | 1406(1) | - | - |
| 1397(1) | - | - | | | | | | |

TABLE II. Gamma-ray energies, relative intensities (corrected for detector efficiency and electron internal conversion and 0 to the strongest transitions in each band), and angular correlation data for the linking transitions of band 1 in $^{134}$Pr and the decoupled band in $^{132}$Pr. Dashed lines indicate that a measurement was not possible through either contamination or low statistics.

| | $^{134}$Pr band 1 | | | $^{132}$Pr decoupled band | |
|---|---|---|---|---|---|
| $E_\gamma$ (keV) | Relative intensity | DCO ratio | $E_\gamma$ (keV) | Relative intensity | DCO ratio |
| 210.6(2) | 0.09(9) | 0.77(14) | 521.8(2) | 0.10(1) | - |
| 245.1(2) | 0.20(2) | 0.81(4) | 577.0(2) | 0.55(2) | 0.56 |
| 339.2(2) | 0.23(2) | 0.74(11) | 596.0(2) | 0.10(1) | 0.66 |
| 610.5(2) | 0.47(3) | 0.98(18) | | | |
| 645.2(2) | 0.35(2) | 1.03(4) | | | |

shown in Fig. 3.

At present, the decay path linking band 2 into the known states in $^{134}$Pr has not been unambiguously assigned. However, it is known that transitions of energies 846 and 254 keV are in coincidence with band 2 and the known low-lying levels of $^{134}$Pr. From the measured intensities in Table I, the decay out of the band is observed to occur over the last two states. The low-lying states fed by band 2 are indicated in Fig. 3 by the dashed lines. For clarity only those low-lying states in $^{134}$Pr fed by bands 1 and 2 are shown in Fig. 3. The $(17^-)$ level is the highest spin state observed to be fed by band 2. The unobserved feeding transitions into this state account for 14% of the intensity of band 2. Other states fed by band 2 are the $(16^-)$ (14%), $(15^-)$ (16%), and $(14^-)$ (11%) states.

## IV. DISCUSSION

### A. Introduction

The properties of the two decoupled bands in $^{134}$Pr are discussed in the following subsections, where they are compared to other decoupled bands in neighboring odd-odd nuclei. All configurations are given for frequencies below crossing points. It should be noted that the quoted configurations include the total $N = 5$ proton ($\pi h_{11/2}$) content except where it is otherwise explicitly stated.

### B. Band 1 in $^{134}$Pr and the $^{132}$Pr band

The dynamic moments of inertia, $\mathcal{J}^{(2)} = dI/d\omega$, of the decoupled bands in $^{132}$Pr, $^{134}$Pm, and band 1 in $^{134}$Pr are very similar [see Fig. 4(a)], suggesting that these bands have the same high-$j$ configurations. Lifetime measurements for the $^{134}$Pm band indicate that the decoupled structure in that nucleus has a quadrupole deformation of $\beta_2$=0.29±0.04 [30]. Cranked Woods–Saxon calculations [22,23] have been performed at this deformation without pairing. These suggest that the configuration for this band is $\pi(h_{11/2})^3 \otimes \nu(f_{7/2},h_{9/2})$, in agreement with the previous assignment [30]. Note that at this deformation the neutron $f_{7/2}$ [530]1/2$^-$ and $h_{9/2}$ [541]1/2$^-$ orbitals are strongly mixed.

Total Routhian surface (TRS) calculations for $^{134}$Pr ($Z$=59 and $N$=75) with the odd proton and neutron

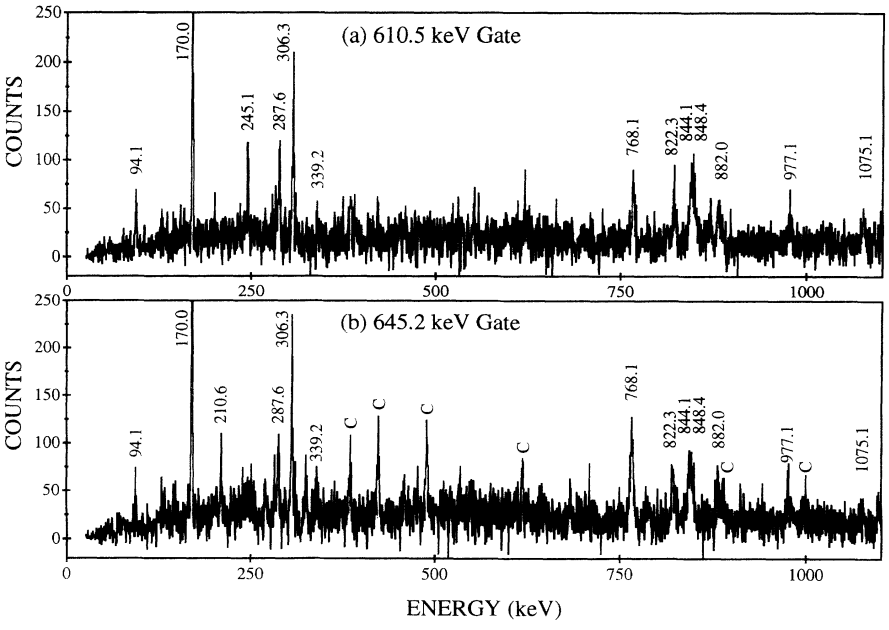


FIG. 2. Coincidence spectra obtained from single gates on the double-gated $\gamma$-$\gamma$ matrix, the transition energies are labeled in keV. (a) The spectrum represents the single 611 keV gate and shows coincidences with the low lying structure in $^{134}$Pr, with the 245 and 339 keV transitions and with transitions of band 1 above the 645 keV transition. (b) The spectrum represents the single 645 keV gate indicating coincidence with band 1, the low lying structure of $^{134}$Pr and the 245 and 339 keV transitions. Other transitions (marked C) are contaminants brought in from the gate and correspond to the oblate band in $^{133}$Ce (Refs. [28,29]).

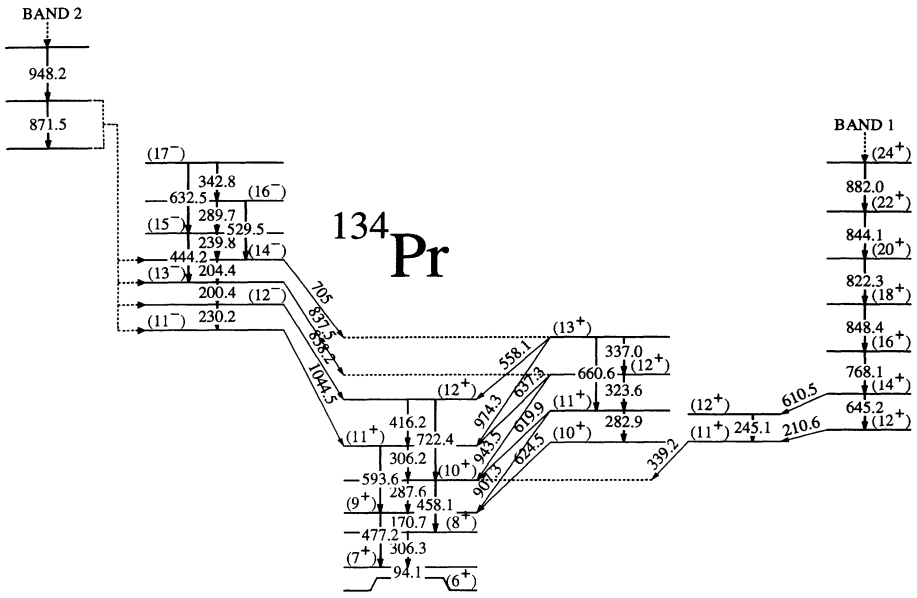


FIG. 3. Partial decay scheme for $^{134}$Pr deduced from the present work. The transition energies are given in keV. For clarity only those states fed by bands 1 and 2 are shown.

occupying the lowest negative-parity negative-signature orbitals indicate that at low frequencies there is an extremely $\gamma$-soft minimum at $\beta_2 \simeq 0.20$, with an absolute minimum at $\gamma \sim +25°$. This corresponds to the $\pi(h_{11/2})^3 \otimes \nu h_{11/2}$ yrast configuration [19]. However, at higher frequencies ($\hbar\omega \geq 0.36$ MeV) the absolute minimum shifts to $\beta_2 \simeq 0.20$ and $\gamma \sim -25°$ (see Fig. 5). This may be associated with the $\pi(h_{11/2})^3 \otimes \nu(f_{7/2},h_{9/2})$ configuration. Using the TRS values for $\beta_2$ and $\gamma$ at high frequency cranked Woods–Saxon calculations were performed without pairing. These calculations, shown in Fig. 6, indicate that the $h_{11/2}$ [541]3/2$^-$ proton and $f_{7/2}$ [530]1/2$^-$ neutron orbitals lie near the Fermi surface. With increasing rotational frequency, these orbitals rapidly approach the Fermi surface, the $f_{7/2}$ [530]1/2$^-$ orbital becoming occupied at intermediate rotational frequencies. It may therefore be expected that this orbital would be populated when the nucleus is produced at high spin. Consequently, a $\pi(h_{11/2})^3 \otimes \nu(f_{7/2},h_{9/2})$ configuration may be expected for band 1.

Similarly, TRS calculations for $^{132}$Pr with the odd proton and neutron occupying the lowest negative-parity negative-signature orbitals indicate a $\gamma$-soft minimum at $\beta_2 \simeq 0.23$ over a wide range of frequencies, $\hbar\omega = 0.0$–0.43 MeV. In this case, the absolute minimum resides at $\gamma \sim 0°$. For this nucleus, cranked Woods-Saxon calculations above $\hbar\omega = 0.3$ MeV show that the $\beta_2 \simeq 0.23$ minimum corresponds to a $\pi(h_{11/2})^3 \otimes \nu(f_{7/2},h_{9/2})$ configuration.

The dynamic moments of inertia for the decoupled bands in $^{132,134}$Pr and band 1 in $^{134}$Pm show evidence of a band crossing at $\hbar\omega \sim 0.4$ MeV, see Fig. 4. The experimental alignment [31] for band 1 in $^{134}$Pr is presented in Fig. 7 as a function of rotational frequency. This plot was produced using Harris parameters of $\mathcal{J}_0 = 11.7\hbar^2$ MeV$^{-1}$ and $\mathcal{J}_1 = 29.0\hbar^4$ MeV$^{-3}$ [19], obtained by fitting levels above the 8$^+$ state of the yrast band in $^{134}$Pr. From these data, the experimental alignment gain has been deduced to be approximately $7\hbar$. In order to try to identify the nature of the aligning particles, cranked Woods–Saxon calculations with pairing were performed with the deformation parameters $\beta_2 = 0.200$, $\beta_4 = 0.015$, and $\gamma = -25°$ for the protons shown in Fig. 8. The proton and neutron pairing gaps were calculated self-consistently at zero rotational frequency and the variation at higher frequencies modelled using the prescription of Ref. [1]. These calculations predict the alignment of two more $h_{11/2}$ protons (the $fg$ crossing) at $\hbar\omega \simeq 0.5$ MeV (Fig. 8). An alignment gain of $\sim 6\hbar$ is predicted by the calculations, which is in reasonable agreement with the experimental alignment, however, the crossing frequency is somewhat higher than

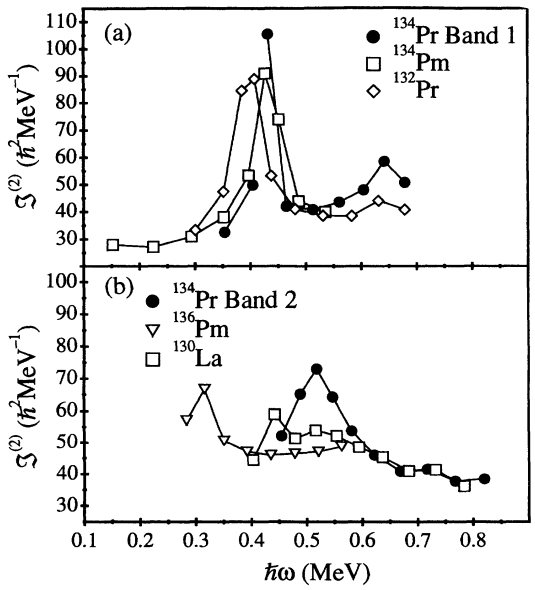


FIG. 4. Dynamic moments of inertia, $\mathcal{J}^{(2)} = dI/d\omega$, plotted as a function of rotational frequency, $\hbar\omega$.

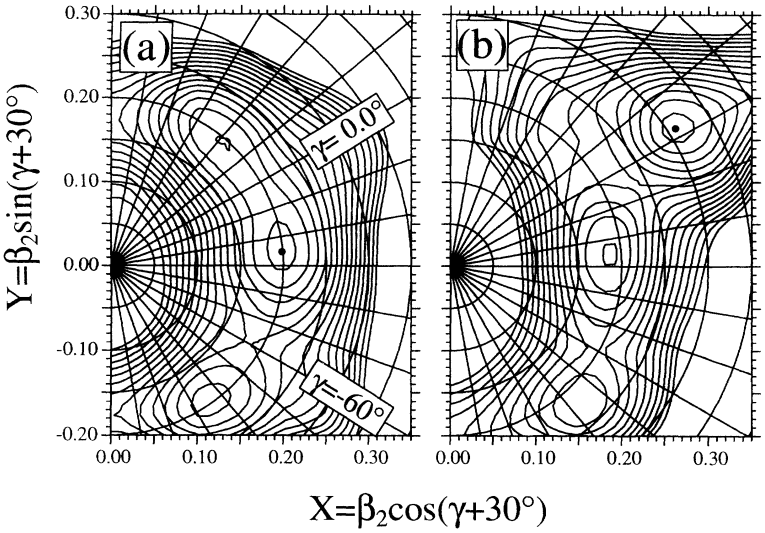


FIG. 5. Total Routhian surface (TRS) calculations for $^{134}$Pr. (a) The odd neutron occupies the favored negative-signature negative-parity orbital and the proton is the favored negative-signature negative-parity state, $\omega$=0.364 MeV/$\hbar$. (b) The odd neutron occupies the favored positive-signature positive-parity orbital and the proton is in the favored negative-signature negative-parity level, $\omega$=0.424 MeV/$\hbar$.

is observed experimentally. In this odd-odd nucleus the valence proton occupying the [541]3/2$^-$ orbital will block the first $h_{11/2}$ proton crossing shown in Fig. 8. This blocking is expected to reduce the pairing strength. Cranked Woods–Saxon calculations performed with a reduced pairing strength, $\Delta'$=0.7$\Delta$($\omega$=0.45 MeV/$\hbar$), lowers the predicted crossing frequency to $\hbar\omega\simeq$0.43 MeV in closer agreement with the observed crossing frequency ($\hbar\omega$=0.41 MeV). Similar calculations, using a pairing interaction reduced by 70%, for the $^{132}$Pr and $^{134}$Pm bands with $\beta_2$=0.23 and $\beta_2$=0.27, respectively, predict crossing frequencies which are in good agreement with the observed crossing frequencies.

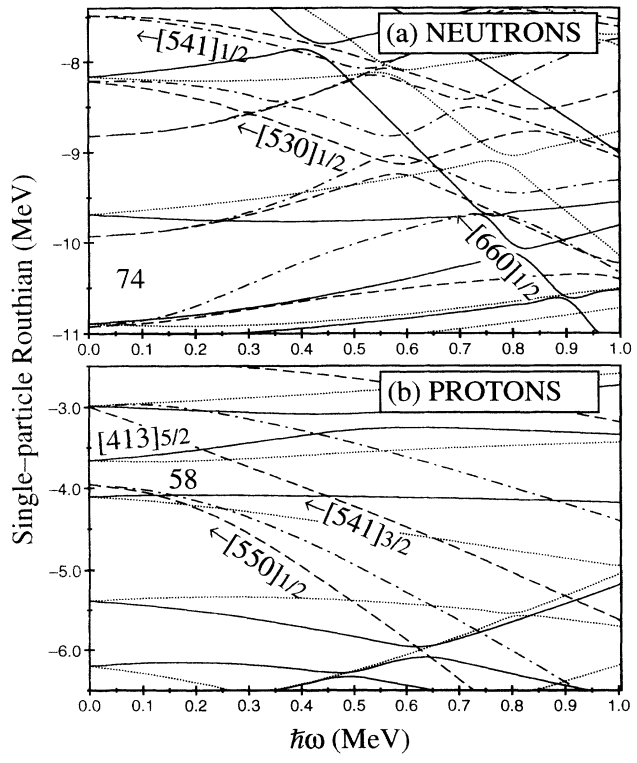


FIG. 6. Single-particle Woods–Saxon Routhian diagrams for (a) neutrons and (b) protons calculated with deformation parameters $\beta_2$=0.200, $\beta_4$=0.015, and $\gamma$=−25°. Signature and parity ($\pi$,$\alpha$) of the levels are indicated in the following way: solid=(+,+$\frac{1}{2}$), dotted=(+,−$\frac{1}{2}$), dot-dashed=(−,+$\frac{1}{2}$), and dashed=(−,−$\frac{1}{2}$).

### C. Band 2

The $\mathcal{J}^{(2)}$ moments of inertia of rotational bands in $^{130}$La [10] and $^{136}$Pm [32] are plotted alongside that of band 2 in $^{134}$Pr; see Fig. 4(b). The similarity of the moments of inertia at high rotational frequency between the $^{130}$La band and band 2 in $^{134}$Pr suggests that the two structures have the same configurations. The main difference is the large hump around $\hbar\omega\simeq$0.5 MeV in $^{134}$Pr, which may be indicative of an additional alignment occurring in this nucleus. Both the $^{130}$La and

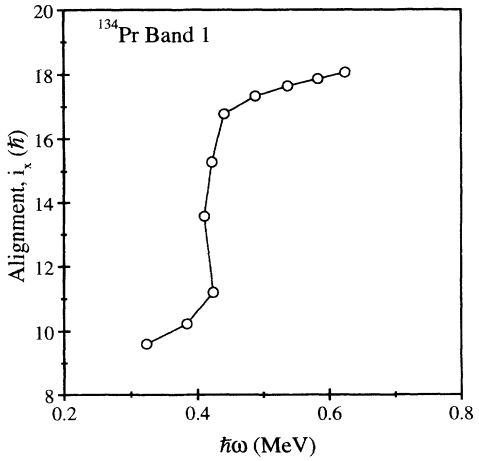


FIG. 7. Experimental alignment, $i_x$, plotted as a function of rotational frequency, $\hbar\omega$ for band 1 in $^{134}$Pr.

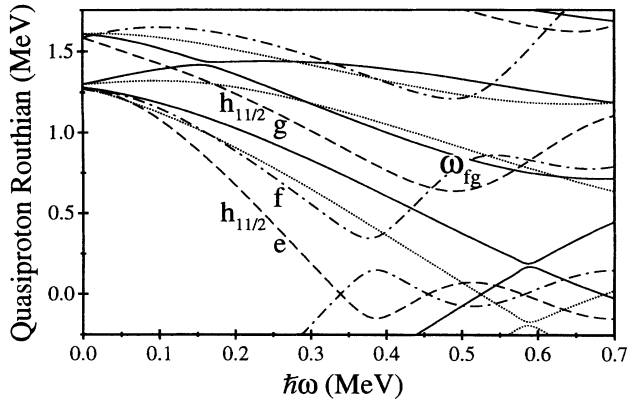


FIG. 8. Cranked Woods–Saxon Routhian diagrams with pairing for protons in $^{134}$Pr. The deformation parameters used were $\beta_2$=0.200, $\beta_4$=0.015, and $\gamma$=−25°. Signature and parity ($\pi$,$\alpha$) of the levels are indicated as for Fig. 6

$^{136}$Pm structures have been associated with the $\nu i_{13/2}$ deformation driving intruder orbital. TRS calculations for the odd neutron occupying the favored positive-signature positive-parity orbital and the proton in the favored negative-signature negative-parity level in $^{134}$Pr are shown in Fig. 5(b). These indicate a minimum at $\beta_2 \simeq 0.31$, $\gamma \simeq 2°$. Using these values of $\beta_2$ and $\gamma$, cranked Woods–Saxon calculations have been performed without pairing. These calculations predict that the strongly down-sloping $i_{13/2}$ [660]$\frac{1}{2}^+$ neutron orbital lies near the Fermi surface, Fig. 9, and occupation of this orbital is expected to give rise to highly deformed bands. The odd proton is expected to occupy the favored $h_{11/2}$ signature ($\alpha=-\frac{1}{2}$) level. A configuration of $\pi(h_{11/2})^3 \otimes \nu i_{13/2}$ is therefore suggested by these calculations for the band in $^{134}$Pr. Similar calculations for the nuclei $^{130}$La and $^{136}$Pm indicate that the highly deformed structure in $^{130}$La has the same configuration while that in $^{136}$Pm has a $\pi(h_{11/2})^5 \otimes \nu i_{13/2}$ configuration. This would account for the similarity of the $\mathcal{J}^{(2)}$ moment of inertia of band 2 with that of the highly deformed band in $^{130}$La. It is not clear from the present calculations whether the additional two $h_{11/2}$ protons can account for the difference in the moments of inertia of the highly deformed band in $^{136}$Pm and the equivalent bands in $^{130}$La and $^{134}$Pr (band 2).

Paired cranked Woods–Saxon calculations with $\beta_2$=0.31, $\beta_4$=0.02, and $\gamma$=2° were performed for both neutrons and protons. These indicate (Fig. 10) a complex alignment pattern involving pairs of $h_{11/2}$ and ($f_{7/2}$,$h_{9/2}$) neutrons at $\hbar\omega \simeq 0.5$ and $\hbar\omega \simeq 0.4$, respectively (at these deformations the $f_{7/2}[530]1/2^-$ orbital is strongly mixed with the $h_{9/2}[541]1/2^-$ orbital). Also the alignment of a pair of $h_{11/2}$ protons may be expected to occur at a frequency of $\hbar\omega \simeq 0.4$ MeV in $^{134}$Pr. Similar calculations

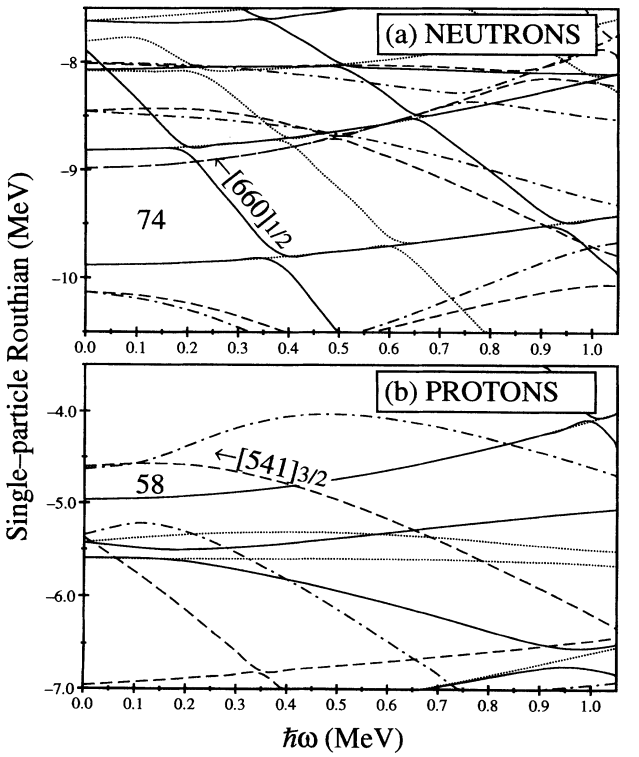


FIG. 9. Single-particle Woods–Saxon Routhian diagrams for (a) neutrons and (b) protons calculated with deformation parameters $\beta_2$=0.310, $\beta_4$=0.015, and $\gamma$=2°. Signature and parity ($\pi$,$\alpha$) of the levels are indicated as for Fig. 6.

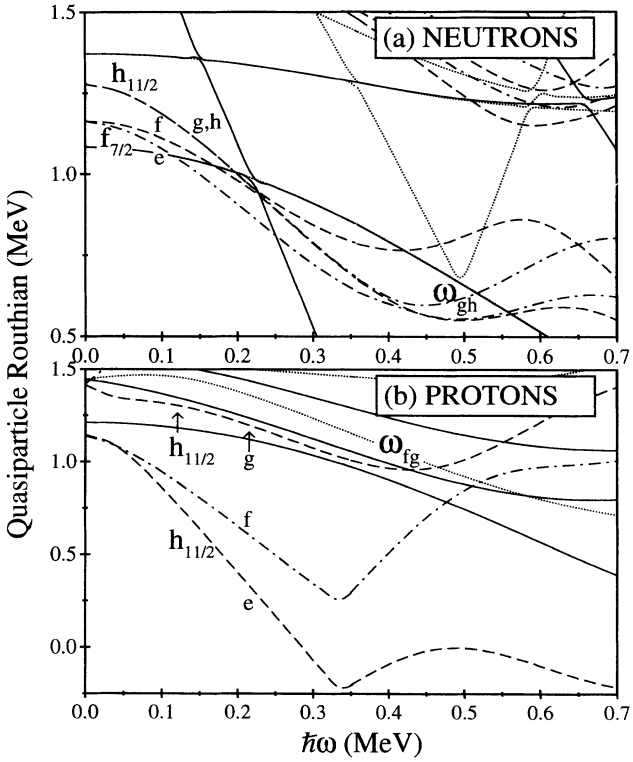


FIG. 10. Cranked Woods–Saxon Routhian diagrams with pairing for (a) neutrons and (b) protons in $^{134}$Pr. The deformation parameters used were $\beta_2$=0.310, $\beta_4$=0.015, and $\gamma$=2°. Signature and parity ($\pi$,$\alpha$) of the levels are indicated as for Fig. 6

for the highly deformed band in $^{130}$La predict that there are alignments of $f_{7/2}$,$h_{9/2}$ neutrons and $h_{11/2}$ protons; however, the $h_{11/2}[514]9/2^-$ neutrons are further above the Fermi surface ($N$=73 compared with $N$=75) and are therefore predicted to align at a somewhat higher rotational frequency, $\hbar\omega\simeq$0.9 MeV. The predicted crossing frequency, $\hbar\omega\sim$0.5 MeV, of the $h_{11/2}[514]9/2^-$ neutrons in $^{134}$Pr corresponds to the frequency at which the enhancement of the $\mathcal{J}^{(2)}$ moment of inertia of band 2 is observed. In this instance calculations with reduced pairing do not significantly alter the crossing frequency. The area under the additional hump in the $\mathcal{J}^{(2)}$ moment of inertia of band 2 between $\omega$ = 0.45 and 0.60 MeV $\hbar^{-1}$ corresponds to $\Delta i_x\simeq 1.5\hbar$ which is indicative of the alignment of a pair of high-$\Omega$ particles. The calculations predict an alignment gain for the $h_{11/2}[514]9/2^-$ neutrons of $\sim 1\hbar$, which agrees well with the experimentally observed value. The good agreement between theory and experiment in this case strongly supports the assignment of the $\pi(h_{11/2})^3 \otimes \nu i_{13/2}$ configuration to band 2.

Finally, the minimum in the TRS calculations for the above configuration [see Fig. 5(b)] is well defined and separated by a large barrier from the lower-deformed minimum. This probably results in a highly fragmented deexcitation process. The lack of observation of linking transitions for this band is therefore consistent with the discussion in the introduction regarding the depopulation mechanism for the high-$j$ intruder bands in this mass region.

## V. CONCLUSION

Two new deformed rotational bands have been observed in the odd-odd nucleus $^{134}$Pr and known decoupled band in $^{132}$Pr has been extended significantly. One of the bands in $^{134}$Pr and the band in $^{132}$Pr are tentatively assigned a $\pi(h_{11/2})^3 \otimes \nu(f_{7/2},h_{9/2})$ configuration for which a deformation of $\beta_2\sim$0.20 and $\gamma\sim -25^\circ$ and $\beta_2\sim$0.23 and $\gamma\sim 0^\circ$ are predicted, respectively, from TRS calculations. Cranked Woods–Saxon calculations with a reduced pairing interaction can reproduce the observed crossing frequencies for these bands using the above deformation parameters. The second band in $^{134}$Pr has been assigned the configuration $\pi(h_{11/2})^3 \otimes \nu i_{13/2}$. This later configuration is expected to result in a more deformed nuclear shape with $\beta_2\sim$0.31 and $\gamma\sim 2^\circ$.

## ACKNOWLEDGMENTS

The Eurogam project is supported by grants from the SERC (U.K.) and the IN2P3 (France). Three of us (A.G., J.G., and D.S.) acknowledge support from the exchange program between CNRS and the Royal Society, while (R.M.C., A.T.S., and J.N.W.) acknowledge financial support of the SERC and K.H. acknowledges financial support from the University of York. We also wish to express our gratitude to Dr. R. Wyss and Dr. W. Nazarewicz for providing the TRS and Woods–Saxon cranking codes. The crew and staff at the Daresbury Laboratory are also thanked.

[1] R. Wyss, J. Nyberg, A. Johnson, R. Bengtsson, and W. Nazarewicz, Phys. Lett. B **215**, 211 (1988).

[2] Y. He, M.J. Godfrey, I. Jenkins, A.J. Kirwan, P.J. Nolan, S.M. Mullins, R. Wadsworth, and D.J.G. Love, J. Phys. G **16**, 657 (1990).

[3] A. J. Kirwan, G.C. Ball, P.J. Bishop, M.J. Godfrey, P.J. Nolan, D.J. Thornley, D.J.G. Love, and A.H. Nelson, Phys. Rev. Lett. **58**, 467 (1987).

[4] D. Bazzacco, F. Brandolini, R. Burch, A. Buscemi, C. Cavedon, D. De Acuna, S. Lunardi, R. Menegazzo, P. Pavan, C. Rossi-Alvarez, M. Sferrazza, R. Zanon, G. de Angelis, P. Bezzon, M.A. Cardona, M. De Poli, G. Maron, M.L. Mazza, D. Napoli, J. Rico, S. Spolaroe, X.N. Tang, G. Vedovato, N. Blasi, I. Castigiloni, G. Falconi, G. LoBianco, P.G. Bizzeti, and R. Wyss, Phys. Lett. B **309**, 235 (1993).

[5] E.M. Beck, F.S. Stephens, J.C. Bacelar, M.A. Deleplanque, R.M. Diamond, J.E. Draper, C. Duyar, and R.J. McDonald, Phys. Rev. Lett. **58**, 2182 (1987).

[6] S.M. Mullins, R. Wadsworth, J.M. O'Donnell, P.J. Nolan, A.J. Kirwan, P.J. Bishop, M.J. Godfrey, and D.J.G. Love, J. Phys. G **13**, L201 (1987).

[7] E.S. Paul, R. Ma, C.W. Beausang, D.B. Fossan, W.F. Piel, Jr., S. Shi, N. Xu, and J.-Y. Zhang, Phys. Rev. Lett. **61**, 42 (1988).

[8] P. Vaska, S. Bhattacharjee, D.B. Fossan, D.R. LaFosse, Y. Liang, H.S. Schnare, K. Starosta, M.P. Waring, I. Hibbert, R. Wadsworth, K. Hauschild, C.W. Beausang, S. Clarke, S.A. Forbes, P.J. Nolan, E.S. Paul, A.T. Semple, S. Mullins, H. Grawe, and K.H. Maier, Phys. Rev. C **50**, 104 (1994).

[9] S.M. Mullins, A. Omar, L. Persson, D. Prévost, J.C. Waddington, H.R. Andrews, G.C. Ball, A. Galindo-Uribarri, V.P. Janzen, D.C. Radford, D. Ward, T.E. Drake, D.B. Fossan, D. LaFosse, P. Vaska, M.P. Waring, and R. Wadsworth, Phys. Rev. C **47**, R2447 (1993).

[10] M.J. Godfrey, Y. He, A.J. Kirwan, P.J. Nolan, D.J. Thornley, S.M. Mullins, and R. Wadsworth, J. Phys. G **15**, L163 (1989).

[11] Y.-X. Luo, J.-Q. Zhong, D.J.G. Love, A.J. Kirwan, M.J. Godfrey, I. Jenkins, P.J. Nolan, S.M. Mullins, and R. Wadsworth, Z. Phys. A **329**, 125 (1988).

[12] P.J. Nolan, A.J. Kirwan, D.J.G. Love, A.H. Nelson, D.J. Unwin, and P.J. Twin, J. Phys. G **11**, L17 (1985).

[13] E.M. Beck, R.J. McDonald, A.O. Macchiavelli, J.C. Bacelar, M.A. Deleplanque, R.M. Diamond, J.E. Draper, and F.S. Stephens, Phys. Lett. B **195** 531 (1987).

[14] R. Wadsworth, D.J.G. Love, Y.-X. Luo, J.-Q. Zhong, P.J. Nolan, P.J. Bishop, M.J. Godfrey, R. Hughes, A.N. James, I. Jenkins, S.M. Mullins, J. Simpson, D.J. Thornley, and K.L. Ying, J. Phys. G **13**, L207 (1987).

[15] P.J. Nolan, Nucl. Phys. **A520**, 657c (1990).

[16] F.A. Beck, Prog. Part. Nucl. Phys. **28**, 443 (1992).

[17] C.W. Beausang, S.A. Forbes, P. Fallon, P.J. Nolan, P.J. Twin, J.N. Mo, J.C. Lisle, M.A. Bentley, J. Simpson, F.A. Beck, D. Curien, G. deFrance, G. Duchêne, and D. Popescu, Nucl. Instrum. Methods **A 313**, 37 (1992).

[18] J.N. Wilson, P.J. Nolan, C.W. Beausang, R.M. Clark, S.A. Forbes, A. Gizon, J. Gizon, K. Hauschild, I.M. Hibbert, E.S. Paul, D. Santos, J. Simpson, A.T. Semple, and

R. Wadsworth, Phys. Rev. Lett. (to be published).
[19] C.M. Petrache, G. de Angelis, D. Bucurescu, M. Ivascu, D. Bazzacco, and S. Lunardi, Z. Phys. A **344**, 227 (1992).
[20] C.M. Petrache, G. de Angelis, D. Bucurescu, M. Ivascu, C.A. Ur, D. Bazzacco, S. Lunardi, and R. Wyss (private communication).
[21] S. Shi, C.W. Beausang, D.B. Fossan, R. Ma, E.S. Paul, N. Xu, and A.J. Kreiner, Phys. Rev. C **37**, 1478 (1988).
[22] W. Nazarewicz, J. Dudek, R. Bengtsson, T. Bengtsson, and I. Ragnarsson, Nucl. Phys. **A435**, 397 (1985).
[23] S. Ćwiok, J. Dudek, W. Nazarewicz, J. Skalaski, and T. Werner, Com. Phys. Commun. **46**, 379 (1987).
[24] W. Nazarewicz, R. Wyss, and A. Johnson, Nucl. Phys. **A503**, 285 (1989).
[25] K.S. Krane, R.M. Steffen, and R.M. Wheeler, Nucl. Data Tables **A11**, 351 (1973).
[26] C.W. Beausang, L. Hildingsson, E.S. Paul, W.F. Piel, Jr., N. Xu, and D.B. Fossan, Phys. Rev. C **36**, 1810 (1987).
[27] F. Rösel, H.M. Fries, K. Alder, and H.C. Pauli, Atomic Data Nuclear Data Tables **21**, 109 (1978).
[28] R. Ma, E.S. Paul, C.W. Beausang, S. Shi, N. Xu, D.B. Fossan, Phys. Rev. C **36**, 2322 (1987).
[29] J. Nyberg, A. Ataç, M. Sugawara, A. Virtanen, S. Forbes, M. Metcalfe, S.M. Mullins, E.S. Paul, P.H. Regan, R. Wadsworth, and D. Santonocito, The Niels Bohr and NORDITA Research Activity Report, 1990, p. 63.
[30] R. Wadsworth, S.M. Mullins, P.J. Bishop, A.J. Kirwan, M.J. Godfrey, P.J. Nolan, and P.H. Regan, Nucl. Phys. **A526**, 188 (1991).
[31] R. Bengtsson and S. Frauendorf, Nucl. Phys. **A327**, 139 (1978).
[32] M.A. Riley, T. Petters, J. Shick, J. Doring, J.W. Holcomb, G.D. Johns, T.D. Johnson, O.N. Tekyi-Mensah, S.L. Tabor, P.C. Womble, V.A. Wood, C. Baktash, M.L. Halbert, D.C. Hensley, I.Y. Lee, R.J. Charity, D.G. Sarantites, L.L. Wittmer, and J. Simpson, Phys. Rev. C **47**, R441 (1993).